nuclear fusion
IAEA

PAPER

Surface modification of F82H steel exposed to low energy, high flux He plasmas

To cite this article: Yu-Ping Xu *et al* 2017 *Nucl. Fusion* **57** 056038

View the article online for updates and enhancements.

Related content

- Surface modification and deuterium retention in reduced activation ferritic martensitic steels exposed to low-energy, high flux D plasma and D2 gas
V Kh Alimov, Y Hatano, K Sugiyama et al.
- Blister bursting and deuterium bursting release from tungsten
W.M. Shu, E. Wakai and T. Yamanishi
- Erosion and deuterium retention of CLF-1 steel exposed to deuterium plasma
L Qiao, P Wang, M Hu et al.

Recent citations

- Helium self-trapping and diffusion behaviors in deformed 316L stainless steel exposed to high flux and low energy helium plasma
Yihao Gong *et al*
- Helium, hydrogen, and fuzz in plasma-facing materials
Karl D Hammond

This content was downloaded from IP address 211.86.158.31 on 22/05/2018 at 08:26

IOP Publishing | International Atomic Energy Agency Nuclear Fusion

Nucl. Fusion **57** (2017) 056038 (8pp) https://doi.org/10.1088/1741-4326/aa635d

Surface modification of F82H steel exposed to low energy, high flux He plasmas

Yu-Ping Xu[1,2], Hai-Shan Zhou[1], Y.K. Martin Peng[1,2], Tao Lu[1], Xiao-Chun Li[1], Feng Liu[1], Jing Wang[1,2], Hao-Dong Liu[1,2], Yi-Ming Lyu[1,2] and Guang-Nan Luo[1,2,3,4]

[1] Institute of Plasma Physics, Chinese Academy of Sciences, Hefei 230031, People's Republic of China
[2] University of Science and Technology of China, Hefei 230026, People's Republic of China
[3] Hefei Center for Physical Science and Technology, Hefei 230031, People's Republic of China
[4] Hefei Science Center of Chinese Academy of Science, Hefei 230027, People's Republic of China

E-mail: gnluo@ipp.ac.cn

Received 23 April 2016, revised 21 February 2017
Accepted for publication 28 February 2017
Published 4 April 2017

Abstract

Polished F82H steel samples were exposed to He plasmas with an ion incident energy of ~80 eV at 773–873 K to three central exposure fluences: 6×10^{24}, 1×10^{25} and 4×10^{25} He m^{-2}. Pinholes with diameters less than 70 nm are densely distributed on all exposed samples, resulting from the formation and bursting of blisters. Further, tendril-like features in maze-like patterns on the top of terrace-like ridges are visible for the sample exposed to 4×10^{25} He m^{-2} in the beam center. EDS indicates that the tendrils are tungsten enriched. Voids with different sizes and shapes with a depth up to 3.5 μm are observed across the sample exposed to 1×10^{25} He m^{-2}. Over the area exposed to a fluence of up to 2×10^{24} He m^{-2}, variations of wavy morphology and blisters are also observed, which could correlate with the crystallographic orientation at the surface. These He pre-exposed F82H steel samples were subsequently subjected to the conditions near the plasma edge in the EAST tokamak for 367 D plasma pulses of varied durations. It is found that the tendril-like features are partially destroyed by these plasma exposures. These results suggest that the properties of the material likely undergo substantial changes due to expected plasma exposure in a tokamak environment. The bursting of blisters and erosion of W-enriched tendrils would introduce additional impurities that could negatively influence the operation of a fusion device.

Keywords: plasma-surface interaction, nanostructured layers, RAFM steels, helium

(Some figures may appear in colour only in the online journal)

1. Introduction

Reduced activation ferritic/martensitic (RAFM) steels such as F82H steels are the primary candidate structural materials for the first wall and blanket in future fusion power plants [1, 2]. In many DEMO design concepts [3, 4], the RAFM steels are supposed to be protected from erosion by a thin layer of tungsten (W) armor. However, considering the fact that W armor could bring issues such as higher cost and technological challenges in bonding W with RAFM steels, bare RAFM steels have been proposed as the plasma facing materials (PFMs) in many blanket concepts for DEMO and commercial reactors [5]. However, there is concern that the PFM's surface morphology will be changed by the plasma irradiation. As a result, the thermal conductivity near the surface and the retention of hydrogen isotopes may be influenced [6]. Hence, it is important to investigate the plasma exposure behaviour of RAFM steels. Recent studies [7] have shown that after exposure to low energy, high flux deuterium (D) plasma, the near-surface layer of steels would be enriched with W owing to different sputtering yields between low-Z and high-Z materials with hydrogen isotope particles. When D ion energy increased to 200 eV, column-like and coral-like structures could be formed at a certain temperature range [8]. The W-enriched layer was expected to reduce the physical sputtering yields of the steels by plasma exposure [7], favouring the idea to use

 © 2017 IAEA, Vienna Printed in the UK

Table 1. Chemical composition of the F82H steel (wt.%) [2]. Reprinted from [16], Copyright 2002, with permission from Elsevier.

Fe	C	Si	Mn	Cr	V	W	N	Ta
Base	0.090	0.100	0.210	7.460	0.150	1.960	0.006	0.023

RAFM steels as PFMs. It should be noted that fusion plasma contains helium (He) as well, which has a lower physical sputtering threshold energy than D. For W as a PFM candidate, the effects of He plasma exposure on W surface modifications are quite different from the effects of hydrogen isotope plasma, such as the formation of He holes/bubbles [9, 10] and a fibre-like nanostructure [11, 12]. At present, He plasma exposure behaviour of RAFM steels has not yet been found in the literature (a post reviewing change can be found in [13]). It is therefore important to investigate the plasma exposure behaviour of RAFM steels.

This article reports the first measurements of RAFM steels exposed to He plasma at temperatures higher than 773 K, which are close to operation temperatures of the first wall in some blanket concepts for DEMO reactors, for example, 823 K–903 K for the He-cooled pebble-bed (I-HCPB) ceramic blanket and 753 K–893 K for the dual-coolant (DC) blanket [14, 15]. The F82H samples were exposed by He plasma to three different fluences. Interesting nanostructures are observed, e.g. W-enriched tendril-like features that form a maze-like pattern on the top of the ridge, wavy morphology and blisters on the sample surfaces. Then, a possible formation mechanism is discussed. In addition, to further characterize the influence of the He plasma exposures on the performance in the tokamak environment, the He pre-exposed F82H samples and a virgin one are exposed to plasmas in the EAST tokamak, and the surface morphology is observed and compared.

2. Experimental

The F82H steel was used in this work, with the chemical composition shown in table 1 [2]. Samples with the dimensions of $10 \times 10 \times 1\,\mathrm{mm}^3$ were cut and first mechanically polished to a mirror finish and then electro-polished in 10 wt.% $HClO_4$ alcoholic solution at ~253 K. Figure 1(*a*) shows the surface morphology of the electro-polished samples before plasma exposure. Figure 1(*b*) is presented to characterize the grain boundaries of original austenite and martensite laths using an Inlens detector, and the white spots reveal precipitates, mainly accumulating at the grain boundaries.

Then the samples were exposed to a low energy, high flux He plasma at the STEP facility in Beihang University [16]. A couple of samples were exposed together side by side in one turn. The center of the plasma beam was located in the middle between the samples. The whole exposure area was about $8 \times 16\,\mathrm{mm}^2$ owing to the sample holder, and for each sample, the exposure area was about $8 \times 8\,\mathrm{mm}^2$. The flux at the beam center area was measured to be 1.8×10^{22} He/m^2/s by a Langmuir probe, and about one third at the very edge of the irradiation zone (~8 mm away from the beam center) owing to the Gaussian distribution of the plasma beam flux, i.e. allowing the study of different fluences on one sample. The ion incident energy was ~80 eV controlled by a negative bias. The sample temperatures were measured to be 773 K–873 K by a thermocouple tightly pressed onto the sample's back side below the center of the plasma beam. There was a temporal variation during each exposure within 100 K because the samples were passively heated by the plasma whose flux fluctuates within a narrow range. The sample holder was water-cooled. As the distance between the edge and the center is very small, during long-time exposure, we believe the temperature gradient existing along the irradiated area is tiny owing to heat conduction. Three sample pairs were exposed to three fluences at the central irradiated area of 6×10^{24}, 1×10^{25} and 4×10^{25} He m^{-2}, respectively.

To further investigate the influence of the He pre-irradiation on the performance during plasma exposure in the tokamak environment, these He plasma exposed samples and a virgin one were subsequently subjected to the conditions near the plasma edge in the EAST tokamak for 367 D plasma pulses of varied durations with a total exposure time of ~2000 s employing the material and plasma evaluation system (MAPES) during the 2015 spring campaign. The sample surfaces were 5 mm behind the limiter and the local electron temperature and density were measured to be $T_e = 5$–10 eV and $n_e = \sim 1 \times 10^{18}$ m^{-3} by a Langmuir probe. Thermocouples were attached to the samples and the measured temperatures varied from 323 K to 623 K due to the heat from the plasmas.

The surface morphology of the samples before and after each step of plasma exposure was investigated by means of scanning electron microscopy (SEM), and the chemical composition of the nanostructure was identified by an energy dispersive spectrometer (EDS) coupled to the SEM. The cross-sections for imaging with SEM were prepared by a focused ion beam (FIB) in a double-beam FIB micro-nano processing apparatus (Helios 600i from FEI Company) with Pt-C deposition probability on the samples to protect the nanostructure layer. The FIB and subsequent SEM (Helios 600i from FEI company) as well as EDS (X-MAX 80 from Oxford Instrument, the analyses software is INCA from Oxford Instrument) were done by WinTech Nano-Technology Services Pte. Ltd.

3. Surface modification of the F82H samples after He plasma exposure

Figure 2 shows the SEM images of the areas of highest fluence on the three samples with different magnifications and tilting after the He plasma exposures. The images show significant surface morphology changes compared with the virgin surface in figure 1. With raising the He irradiation fluence from sample (*a*)–(*c*), the density of nanostructures on the sample surface increases. Pinholes with diameters less than 70 nm are densely distributed on all the samples. For sample (*b*), clear cellular grooves could be seen in the images taken at small magnification with similar dimensions to that of the original austenite grains. High density of tendril-like features

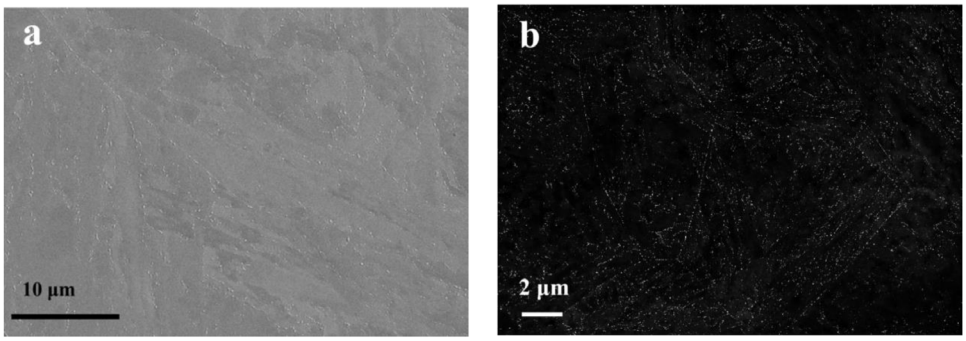

Figure 1. Surface morphology of the electro-polished F82H steel samples before plasma exposure: (*a*) and (*b*) are shown in different contrasts; (*b*) shows grain boundaries of original austenite and martensite laths observed using an inlens detector.

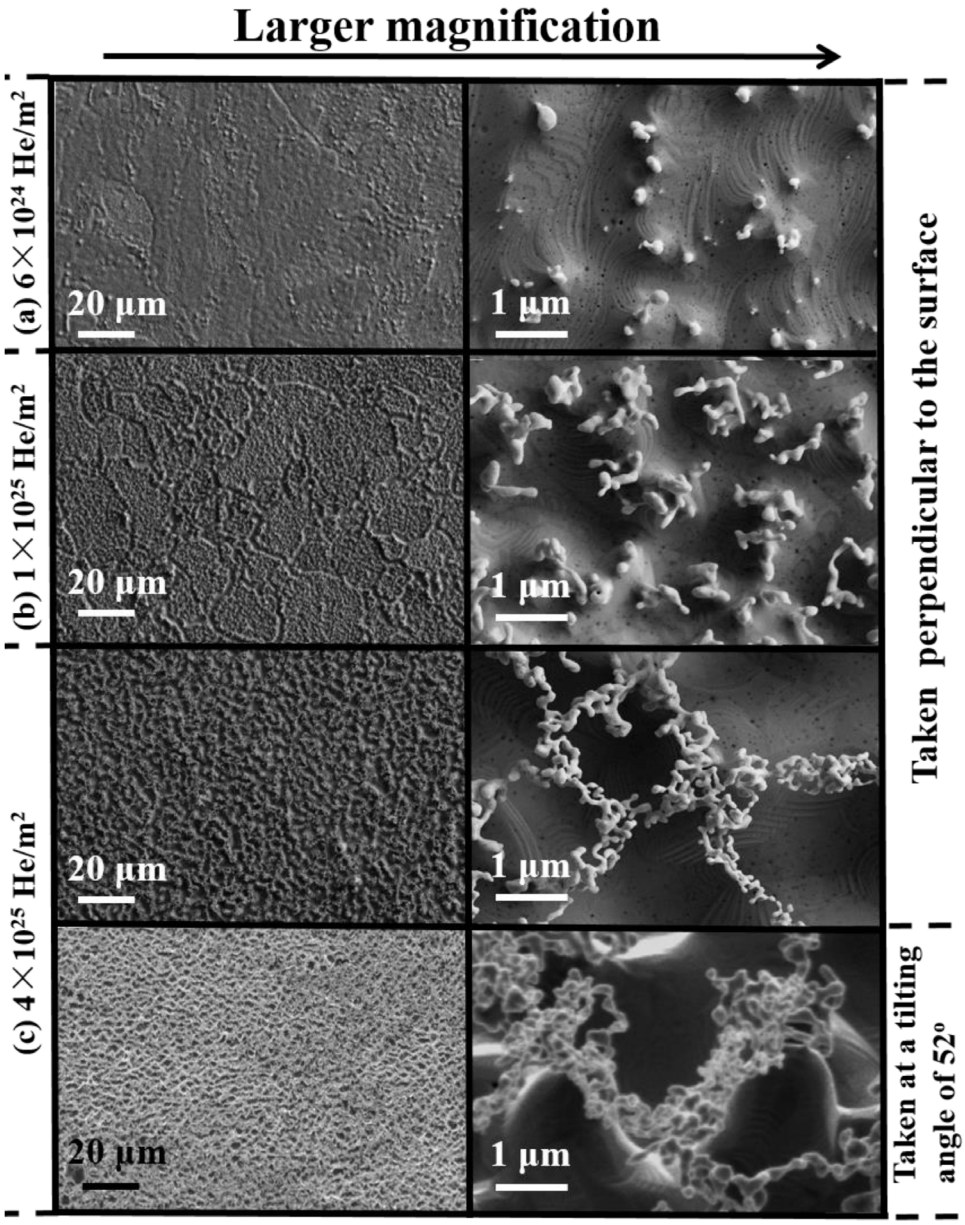

Figure 2. Surface morphology of the area with the highest fluence of the three samples after exposure to fluences of 6×10^{24} He m^{-2}, 1×10^{25} He m^{-2} and 4×10^{25} He m^{-2}, respectively. The He ion energy was 80 eV and the temperatures of the samples were measured to be 773 K–873 K. (*a*) 6×10^{24} He m^{-2}, (*b*) 1×10^{25} He m^{-2}, (*c*) 4×10^{25} He m^{-2}.

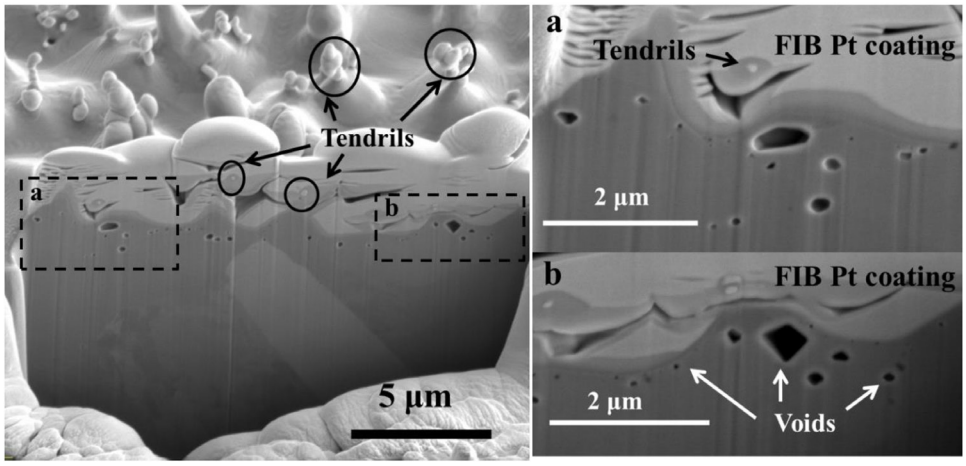

Figure 3. SEM images on cross-sections of the sample exposed to pure He plasma. He ion energy and fluence are 80 eV and 1×10^{25} He m^{-2}, respectively. The temperatures of the samples were measured to be 773 K–873 K.

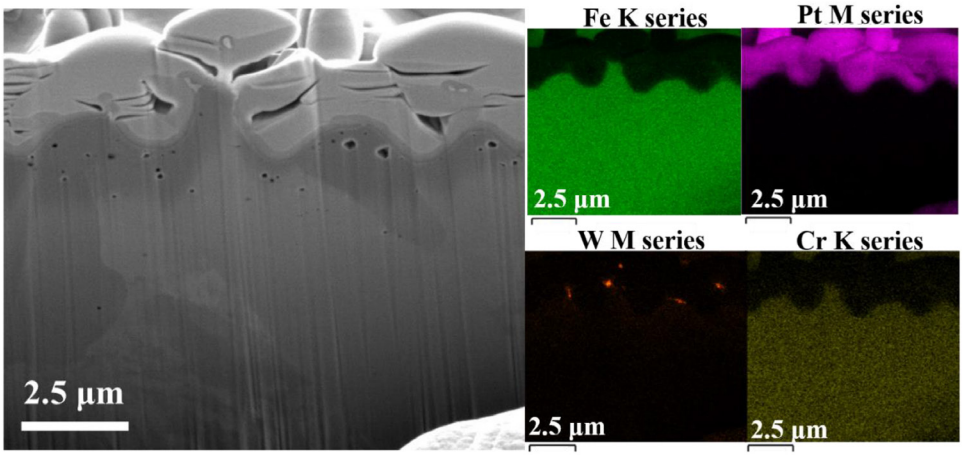

Figure 4. EDS element mapping on the cross-section. He ion energy and fluence are 80 eV and 1×10^{25} He m^{-2}, respectively. The temperatures of the samples were measured to be 773 K–873 K.

are observed on sample (*c*) with the highest fluence, while the grooves are not observable anymore. When imaged at a tilting angle of 52°, the tendril-like features that form a maze-like pattern are clearly visible on the terrace-like ridges.

To further investigate the effects of He, SEM images on cross-sections of the sample were taken on the sample exposed to 1×10^{25} He m^{-2}, as shown in figure 3. Voids with different sizes and shapes can be found in the sample with a depth up to 3.5 μm. In the near surface regions, small voids are densely distributed. Tendrils are visible in the top part of figure 3. The position of the tendrils visible in the top part seems to be affected slightly by the Pt-C deposition and FIB cutting. The morphology and position of the tendrils can be seen clearly in figure 2. Figure 4 shows the element distribution on the cross-section, which indicates that the tendrils visible in the top part of figure 3 are enriched in W.

An interesting point is that on the ridges, which are below the W-enriched tendrils, clear waves can be seen, making the ridges terrace-like, as shown in figure 2. To characterize the terrace-like structure, we tried to find an area that was not shadowed by the tendrils on the samples with the least fluence (shown in figure 5), which probably reveals the initial stage of the tendrils. The irradiation fluence for this area is about 4×10^{24} He m^{-2}.

Another interesting phenomenon is blistering at the edge of the exposed area of the 6×10^{24} He m^{-2} sample (shown in figure 6); the fluence of this area at the edge of the exposure spot is about 2×10^{24} He m^{-2}. Two broad morphology categories are identified, i.e. wavy morphology as described in the last paragraph, and blisters with a diameter up to 1.2 μm. In figure 6(*b*), various bursting with details are shown.

4. Discussion

Due to the lack of studies on He plasma exposure of RAFM steels, we herein try to make comparison with similar experiments, e.g. D plasma exposure of the F82H steel and He plasma exposure of W materials. It has been reported that after exposure of the F82H steel to 200 eV high flux D plasma, a 300 nm thick column-like structure was observed at the irradiation temperature of 460 K, while a 2 μm thick coral-like structure appeared when the irradiation temperature was increased to 770 K [8]. For W, a widely investigated phemonenon is that after exposure to >20–30 eV He plasma for a sufficiently long time, fibre-like structures are found to grow from bulk W when simultaneously heated to ~900 K–2000 K [11, 12, 17].

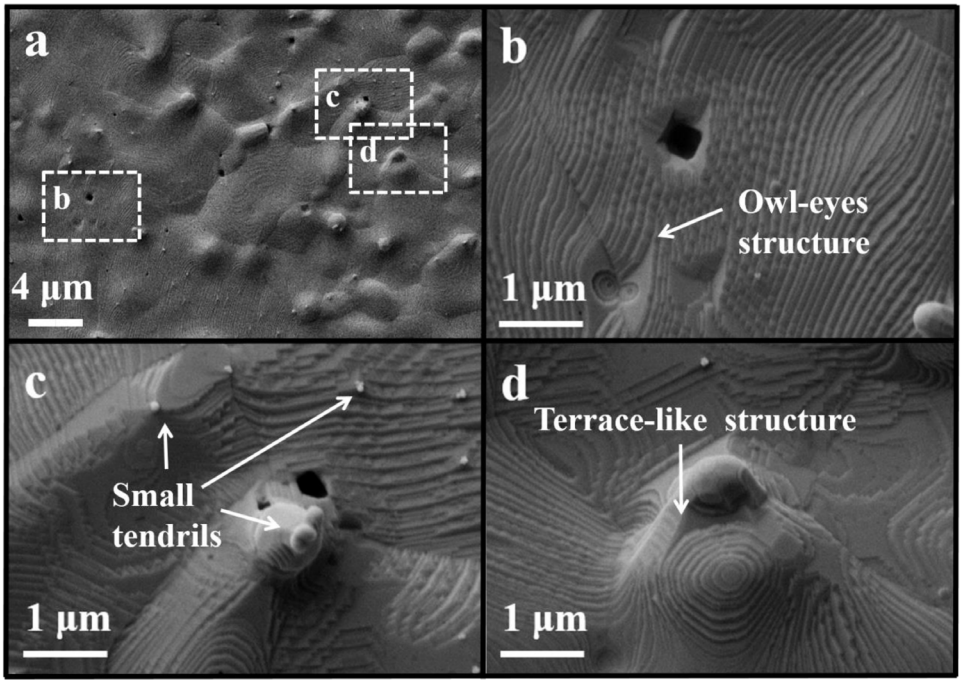

Figure 5. SEM images of the areas with a terrace-like structure and no big tendrils and no 70 nm pinholes. The shown area was exposed to about 4×10^{24} He m^{-2}. *(b)*, *(c)*, *(d)* show areas in *(a)* with characteristic features at larger magnification.

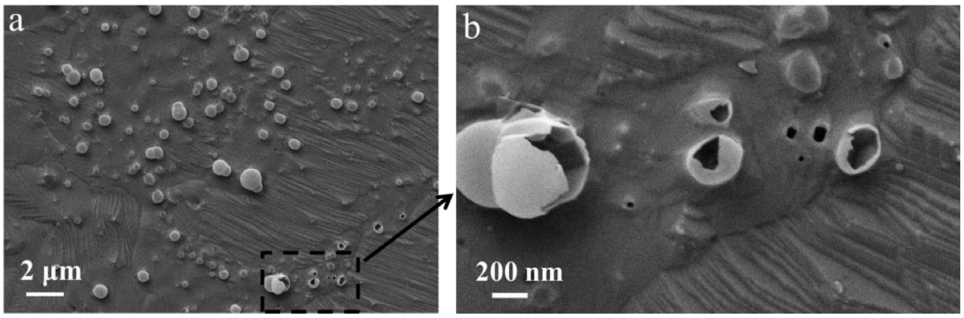

Figure 6. SEM images of the areas with spatial distribution of blisters and waves. The shown area was exposed to about 3×10^{24} He m^{-2}. *(b)* shows a zone in *(a)* with bursting blisters at larger magnification.

In our case, as shown in figure 2, the nanostructures on the F82H steel surface after exposure to 80 eV He plasma at 773 K–873 K include tendrils and terrace-like ridges. For sample (c), the tendril-like features that form a maze-like pattern are clearly shown on terrace-like ridges, which are quite different from the reported nanostructures on F82H steels after D plasma exposure and bulk W after He plasma exposure. Figure 4 clearly presents the W enrichment. The enrichment of W can be explained by preferential sputtering between low-*Z* and high-*Z* materials with He particles [18]. Alimov *et al* investigated the F82H steel morphology after D plasma exposure [8], and found that the morphology of the W-enriched layer varied at different temperatures, implying the diffusion of W atoms may be the reason for W accumulation. As the surface diffusion is, in general, much faster than lattice diffusion [19], the active surface diffusion of W atoms may play an important role in the formation of W-enriched branches in our case.

In figure 3, the cross-section morphology is shown. The distance between the tendrils and the ridge bottom is about 3 μm. Using the sputtering yield data of Fe with 80 eV He ions, ~0.02 atom/ion [20], the eroded depth of pure Fe exposed to 1×10^{25} He m^{-2} can be estimated as 2.4 μm,

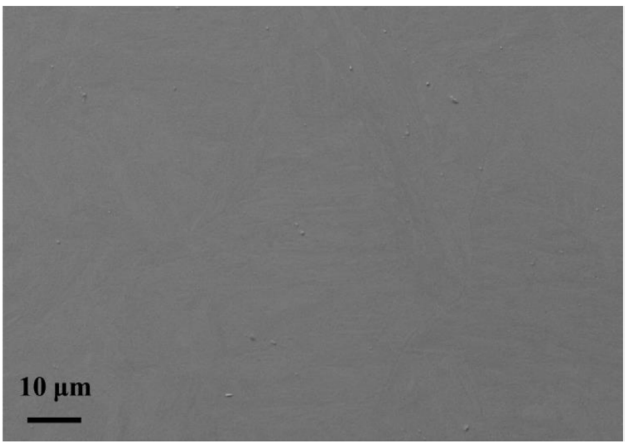

Figure 7. SEM image of the bare F82H steel sample after exposure to 367 D plasma pulses of varied durations in EAST.

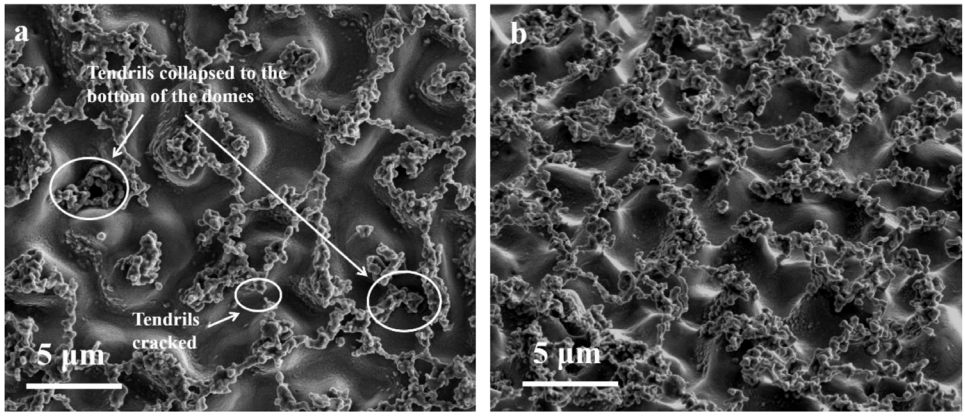

Figure 8. SEM images of the center of the sample after exposure to He plasma to a central fluence of 4×10^{25} He m^{-2} and 367 D plasma pulses of varied durations in EAST. (*a*) taken perpendicular to the surface and (*b*) taken at a tilting angle of 52°.

which fits quite well with the distance from the top of the tendrils to the bottom of the ridges. Except for the sizes of the voids, it should be noted that the depth for the voids is up to 3.5 μm, which is much larger than the implantation depth. Stoller *et al* from Oak Ridge National Laboratory have performed extensive atomistic simulations with a three-body Fe–He potential [21–23]. They found that interstitial He is very mobile and easy to coalesce together to form interstitial clusters. They have calculated the diffusion coefficient of He interstitial clusters. Based on their results, we estimate that the diffusion coefficient of He interstitial clusters (1–6 He atoms) at 773 K–873 K is larger than 1×10^{-9} m^2 s^{-1}. Based on Fick's laws of diffusion, the max diffusion distance for He interstitial clusters can be estimated by $\sqrt{D \times t}$, where t is the diffusion time, and D is the diffusion coefficient [24]. In the case for the sample exposed to 1×10^{25} He m^{-2}, the maximal diffusion distance is up to several hundreds of micrometers. Thus a depth of the voids much higher than the implantation is reasonable.

For the cellular grooves on sample (b) in figure 2, as the dimension of the grooves is comparable to that of the original austenite, the formation of grooves may result from the preferential erosion along the boundaries of the original austenite. Similar grooves have been reported on W at the boundaries after exposure to He ions, and it is concluded that the grooving is thermally induced [25]. Thus the thermal effect may be another possible reason for the formation of grooves.

In figures 2 and 5, clear waves can be seen on the ridges. Wavy morphology has been reported on W after exposure to 25 eV–30 eV He plasma at 1700 K–1800 K [25, 26]. Parish *et al* [25] observed four general morphologies, including wavy morphology, and summarized three possible mechanisms for the observed differences: (1) ion channeling effects, (2) surface energy effects and (3) dislocation loop-punching effects. For the wavy morphology in our experiments, the third mechanism, as also suggested by Ohno *et al* [26], fits best. We believe that dislocation loop punching caused by the growth of He bubbles was driving the surface faceting. As more He atoms accumulate in a bubble, the pressure increases above the equilibrium pressure. The high enough pressure in a He bubble moves the lattices along the slip face. Therefore, the owl-eyes structure in figure 5(*b*) can be explained by dislocation outcrop. Besides, the owl-eyes structure in figure 5(*b*) could also be the remains of voids opened by erosion. The circular waves on the top of ridges as shown in figure 5(*d*) can be explained by the growth of a big bubble in the ridge.

In figure 2, pinholes are densely distributed on all the samples. From figure 6, various bursting features of blisters are observed clearly. As the amount of holes on the samples is large, much attention should be paid as the bursting of blisters may be a significant source for impurities in a fusion device.

In figure 6, the areal distribution of wavy morphology and blisters may be attibuted to the effect of crystallographic orientation. As a comparison, for the He plasma exposed W, it was reported that grains having various orientations can behave differently [25–27]. After exposure to 40 eV He plasma at 1473 K, grains of (0 0 1) orientation have ripple structures decorated with pores, grains of (1 1 0) and (1 1 1) orientations have pores only, and grains of other orientations have different surface morphology (either ripples or pores) depending on their misorientation angle [27]. After the exposure of W to 80 eV He plasma at 1403 K, grain boundary grooving occurs, and four general grain morphologies are observed: smooth, pyramidal, wavy and terraced [25].

5. Exposure of the pre-exposed F82H steel to D plasmas in EAST

During the 2015 spring EAST campaign, these three He plasma irradiated samples and a virgin F82H steel sample were subsequently subjected to the conditions near the plasma edge in the EAST tokamak for 367 D plasma pulses of varied durations with a total plasma exposure time of ~2000 s employing the MAPES [28]. No significant difference was found on the virgin F82H steel sample except that the grain-boundaries and precipitates on the surface disappeared, as shown in figure 7. The tendrils on the 4×10^{25} He m^{-2} sample before EAST plasma exposure were connected like a maze, as previously shown in figure 2. However, after exposure to D plasma in EAST, the tendril-like features with a maze-like pattern were cracked and part of the tendrils collapsed to the bottom of the

ridges while part of the tendrils were missing, as shown in figure 8. The wavy structure vanished. EDS showed that the re-deposited materials on the sample surface were limited with a tiny amount of particles found, which mainly contain Cr, Mn, O and Fe. Besides, the tendril-like features can be seen clearly in figure 8. Thus, the effect of re-deposition can be neglected. As the wavy structure is more sensitive to plasma sputtering than the tendrils because of relatively low W concentration, erosion may be the reason for the vanishing of the wavy structure. As the lost tendrils are W-enriched, careful evaluation should be done owing to possible contamination to the plasma.

6. Conclusion

Surface modification of the F82H steel due to He plasma irradiation was studied in a linear plasma device using He plasmas with an ion incident energy of ~80 eV at 773 K–873 K. Three F82H steel samples were exposed to 6×10^{24}, 1×10^{25} and 4×10^{25} He m^{-2} at the central irradiated area; SEM, EDS and FIB were employed to determine surface/cross-section morphology and chemical composition of the samples. Moreover, to further investigate the influence of He irradiation of surface performance during plasma exposure in a real tokamak environment, the He pre-exposed F82H steel samples were subsequently exposed to the conditions near the plasma edge in the EAST tokamak for 367 D plasma pulses of varied durations employing the MAPES.

Pinholes with diameters less than 70 nm are densely distributed on all the samples exposed to He plasma. On the area exposed to 2×10^{24} He m^{-2}, bursting blisters are observed, which could correlate with the formation of the pinholes. Varied wavy morphology and blisters are also observed. The spatial distribution of wavy morphology and blisters on F82H steel may be attributed to the effect of crystallographic orientation. Tendril-like features are densely distributed on the sample exposed to 4×10^{25} He m^{-2}. When observed at a tilting angle of 52°, the tendril-like features that form a maze-like pattern are visible on top of terrace-like ridges. EDS indicates that the tendrils are W-enriched. On the ridges below the tendril-like features, a terrace-like structure can be seen. Similar wavy morphology has been reported on W after exposure to 25 eV–30 eV He plasma at 1700 K–1800 K by Ohno *et al* [26], where it was proposed that dislocation loop punching caused by the growth of He bubbles was the cause. In addition, voids with different sizes and shapes with a depth up to 3.5 μm are visible on the cross-sections of the areas exposed to 1×10^{25} He m^{-2}.

These results suggest that the near-surface layer of steels is expected to be enriched with W owing to preferential sputtering between low-Z and high-Z materials during plasma exposure, thus the W-enriched layer could reduce the physical sputtering yields of the steels. However, experiments showed that the W-enriched tendrils could be destroyed by the plasma exposure, leading to the increase of the physical sputtering yields of the steel. Besides, it should be noted that blisters and missing tendrils imply additional sources of the impurities into the core plasma, which could be a serious concern for the plasma operation [29]. It was recently reported [19] that He irradiation greatly affects hydrogen isotope behaviour via the formation of He bubble layers that greatly reduce the effective diffusion of hydrogen isotopes. The He voids in F82H steel after He plasma exposure could thus influence the hydrogen isotope retention significantly. Alterations in nanostructures on the F82H steel surface could negatively influence surface-thermal properties of plasma facing components. In view of these new results for such a surface of mixed materials, further experimental investigation and numerical modelling are recommended to reveal the formation and growth process of the surface nanostructure for RAFM steels as a plasma facing material.

Acknowledgments

The authors would like to thank Prof Noriyasu Ohno from Nagoya University for fruitful discussions on the nanostructure formation mechanisms and Prof Yasuhisa Oya from Shizuoka University for providing the F82H steel. The authors would also like to thank Prof Guang-Hong Lu, Dr Jun Wang and Dr Long Cheng from Beihang University for their help in He plasma exposure experiments.

This work is supported by National Magnetic Confinement Fusion Science Program of China (Nos. 2013GB105001, 2015GB109001), the National Natural Science Foundation of China (Nos. 11505232, 11405201), Technological Development Grant of Hefei Science Center of CAS (No. 2014TDG-HSC003), Scientific Research Grant of Hefei Science Center of CAS (No. 2015HSC-SRG054), the Korea Research Council of Fundamental Science and Technology (KRCF) under the international collaboration & research in Asian countries (No. PG1314), the Joint Sino-German research project GZ 765.

References

[1] Baluc N., Gelles D.S., Jitsukawa S., Kimura A., Klueh R.L., Odette G.R., van der Schaaf B. and Yu J. 2007 Status of reduced activation ferritic/martensitic steel development *J. Nucl. Mater.* **367** 33–41

[2] Jitsukawa S. *et al* 2002 Development of an extensive database of mechanical and physical properties for reduced-activation martensitic steel F82H *J. Nucl. Mater.* **307** 179–86

[3] Igitkhanov Y. and Bazylev B. 2012 Evaluation of energy and particle impact on the plasma facing components in DEMO *Fusion Eng. Des.* **87** 520–4

[4] Igitkhanov Y., Bazylev B., Landman I. and Boccaccini L. 2013 Applicability of tungsten/EUROFER blanket module for the DEMO first wall *J. Nucl. Mater.* **438** S440–4

[5] Ueda Y., Tobita K. and Katoh Y. 2003 PSI issues at plasma facing surfaces of blankets in fusion reactors *J. Nucl. Mater.* **313** 32–41

[6] Lindig S., Balden M., Alimov V.K., Yamanishi T., Shu W.M. and Roth J. 2009 Subsurface morphology changes due to deuterium bombardment of tungsten *Phys. Scr.* **138** 014040

[7] Sugiyama K., Roth J., Alimov V.K., Schmid K., Balden M., Elgeti S., Koch F., Höschen T., Baldwin M. and

Doerner R. 2015 Erosion study of Fe–W binary mixed layer prepared as model system for RAFM steel *J. Nucl. Mater.* **463** 272–5
[8] Alimov V.K., Hatano Y., Sugiyama K., Balden M., Höschen T., Oyaidzu M., Roth J., Dorner J., Fußeder M. and Yamanishi T. 2014 Surface modification and deuterium retention in reduced activation ferritic martensitic steels exposed to low-energy, high flux D plasma and D2 gas *Phys. Scr.* **2014** 014049
[9] Dai N., Ye M.Y., Ohno N. and Takamura S. 2004 Formation mechanism of bubbles and holes on tungsten surface with low-energy and high-flux helium plasma irradiation in NAGDIS-II *J. Nucl. Mater.* **329–33** 1029–33
[10] Nishijima D., Ye M.Y., Ohno N. and Takamura S. 2003 Incident ion energy dependence of bubble formation on tungsten surface with low energy and high flux helium plasma irradiation *J. Nucl. Mater.* **313–6** 97–101
[11] Takamura S., Miyamoto T. and Ohno N. 2012 Effects of fibre-form nanostructures on particle emissions from a tungsten surface in plasmas *Nucl. Fusion* **52** 123001
[12] Takamura S., Ohno N., Nishijima D. and Kajita S. 2006 Formation of nanostructured tungsten with arborescent shape due to helium plasma irradiation *Plasma Fusion Res.* **1** 051
[13] Nishijima D., Baldwin M.J., Doerner R.P., Tanigawa H., Wang P. and Yu J.H. 2016 Sputtering properties of RAFM steels under high-flux He plasma exposure *Nucl. Mater. Energy* at press (https://doi.org/10.1016/j.nme.2016.08.019)
[14] Giancarli L., Ferrari M., Futterer M.A. and Malang S. 2000 Candidate blanket concepts for a European fusion power plant study *Fusion Eng. Des.* **49–50** 445–56
[15] Konishi S., Nishio S., Tobita K. and Team D.D. 2002 DEMO plant design beyond ITER *Fusion Eng. Des.* **63–4** 11–7
[16] Liu F., Xu Y., Zhou H., Zhao S., Li B., Lyu G., Yuan Y., Hao T. and Luo G. 2015 Exposure of equal-channel angular extruded tungsten to deuterium plasma *Plasma Sci. Technol.* **17** 595–600
[17] Petty T.J., Baldwin M.J., Hasan M.I., Doerner R.P. and Bradley J.W. 2015 Tungsten 'fuzz' growth re-examined: the dependence on ion fluence in non-erosive and erosive helium plasma *Nucl. Fusion* **55** 093033
[18] Andersen H.H. and Bay H.L. 1981 *Sputtering by Particle Bombardment* I (Berlin: Springer) pp 145–218
[19] Ueda Y., Peng H.Y., Lee H.T., Ohno N., Kajita S., Yoshida N., Doerner R., De Temmerman G., Alimov V. and Wright G. 2013 Helium effects on tungsten surface morphology and deuterium retention *J. Nucl. Mater.* **442** S267–72
[20] Yamamura Y. and Tawara H. 1996 Energy dependence of ion-induced sputtering yields from monatomic solids at normal incidence *At. Data Nucl. Data Tables* **62** 149–253
[21] Seletskaia T., Osetsky Y.N., Stoller R.E. and Stocks G.M. 2006 Calculation of helium defect clustering properties in iron using a multi-scale approach *J. Nucl. Mater.* **351** 109–18
[22] Stewart D., Osetskiy Y. and Stoller R. 2011 Atomistic studies of formation and diffusion of helium clusters and bubbles in BCC iron *J. Nucl. Mater.* **417** 1110–4
[23] Stoller R.E., Golubov S.I., Osetsky N., Kamenski P.J. and Seletskaia T. 2010 Implementation of a Fe–He 3-body interatomic potential *Phil. Mag.* **90** 923–34
[24] Crank J. 1956 The mathematics of diffusion *Math. Gaz.* **8** 1–10
[25] Parish C.M., Hijazi H., Meyer H.M. and Meyer F.W. 2014 Effect of tungsten crystallographic orientation on He-ion-induced surface morphology changes *Acta Materialia* **62** 173–81
[26] Ohno N., Hirahata Y., Yamagiwa M., Kajita S., Takagi M., Yoshida N., Yoshihara R., Tokunaga T. and Tokitani M. 2013 Influence of crystal orientation on damages of tungsten exposed to helium plasma *J. Nucl. Mater.* **438** S879–82
[27] El-Atwani O., Gonderman S., Efe M., De Temmerman G., Morgan T., Bystrov K., Klenosky D., Qiu T. and Allain J.P. 2014 Ultrafine tungsten as a plasma-facing component in fusion devices: effect of high flux, high fluence low energy helium irradiation *Nucl. Fusion* **54** 083013
[28] Ding F. *et al* 2014 Overview of plasma-material interaction experiments on EAST employing MAPES *J. Nucl. Mater.* **455** 710–6
[29] Rubel M., Cecconello M., Malmberg J., Sergienko G., Biel W., Drake J R., Hedqvist A., Huber A. and Philipps V. 2001 Dust particles in controlled fusion devices: morphology, observations in the plasma and influence on the plasma performance *Nucl. Fusion* **41** 1087